

Carbon Nanotubes as Cooper Pair Beam Splitters.

L.G. Herrmann^{1,2,5}, F. Portier³, P. Roche³, A. Levy Yeyati⁴, T. Kontos^{1,2*} and C. Strunk⁵

¹*Ecole Normale Supérieure, Laboratoire Pierre Aigrain,
24, rue Lhomond, 75231 Paris Cedex 05, France*

²*CNRS UMR 8551, Laboratoire associé aux universités Pierre et Marie Curie et Denis Diderot, France*

³*Service de physique de l'état Condensé, CEA, 91192 Gif-sur-Yvette, France.*

⁴*Departamento de Física Teórica de la Materia Condensada C-V,
Universidad Autónoma de Madrid, E-28049 Madrid, Spain.*

⁵*Institut für experimentelle und angewandte Physik,
Universität Regensburg, Universitätsstr.31, 93040 Regensburg, Germany.*

(Dated: November 2, 2018)

We report on conductance measurements in carbon nanotube based double quantum dots connected to two normal electrodes and a central superconducting finger. By operating our devices as beam splitters, we provide evidence for Crossed Andreev Reflections *tunable in situ*. This opens an avenue to more sophisticated quantum optics-like experiments with spin entangled electrons.

PACS numbers: 73.23.-b,73.63.Fg

Quantum optics has been an important source of inspiration for many recent experiments in nanoscale electric circuits[1, 2]. One of the basic goals is the generation of entangled electronic states in solid state systems. Superconductors have been suggested as a natural source of spin entanglement, due to the singlet pairing state of Cooper pairs. One important building block required for the implementation of entanglement experiments using superconductors is a Cooper pair beam splitter which should split the singlet state into two different electronic orbitals [3, 4].

The basic mechanism for converting Cooper pairs into quasiparticles is the Andreev reflection in which an originally quantum coherent electron pair in the singlet spin state is produced at an interface between a superconductor and a normal conductor. Conventional Andreev Reflections (AR) are local and cannot readily be used to create bipartite states[5, 6]. It has been suggested to make use of electron-electron interactions[6, 7, 8, 9, 10, 11, 12, 13], spin filtering [14] or anomalous scattering in graphene [15] to promote Cooper pair splitting i.e. the Crossed Andreev Reflection (CAR) process.

In this letter, we show that Coulomb interactions as well as size quantization can favor the CAR processes in carbon nanotubes. We use a double quantum dot geometry where the nanotube is connected to two normal electrodes and a central superconducting finger. By operating our device as a beam splitter (i.e. biasing the central superconducting electrode), we find that there is a finite current flowing from the superconducting electrode to the left (L) arm and the right (R) arm for a bias voltage smaller than the energy gap of the superconductor, which demonstrates Cooper pair injection. This subgap current is enhanced when we tune the device to the degeneracy

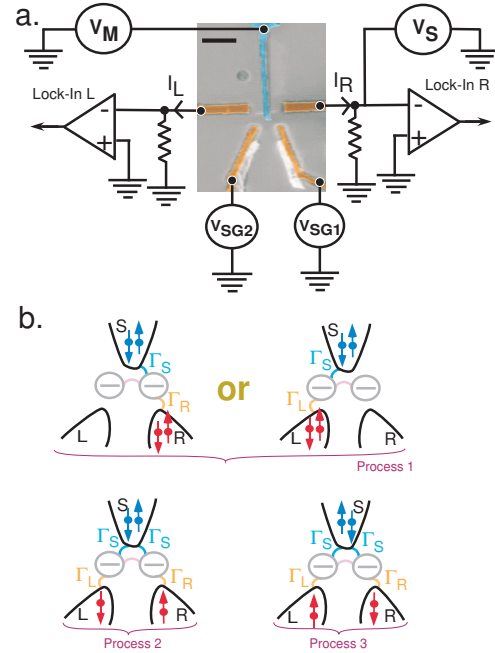


FIG. 1: a. SEM image of a typical Cooper pair splitter device in false colors with the two biasing schemes sketched. The bar is $1\mu m$. A central superconducting electrode is connected to two quantum dots engineered in the same single wall carbon nanotube (in purple) which bridges between electrodes L and R. b. The elementary processes which carry current in the superconducting (S) state. In addition to the conventional local Andreev Reflection process, the Crossed Andreev Reflection can occur in which a Cooper pair is split in the two quantum dots. The relative probability of each of these processes can be inferred from the topology of the beam splitter.

points of the double dot with the help of capacitively coupled side gate electrodes. This enhancement together with the dependence of the asymmetry of transport in the superconducting state with respect to the normal state provide evidence for Crossed Andreev Reflections *tun-*

*To whom correspondence should be addressed: kontos@lpa.ens.fr

able *in situ*, in contrast to the weakly interacting metallic case[16, 17]. These conclusions are supported by theoretical calculations based on a straightforward modeling of the device.

We use chemical vapor deposition to fabricate our SWNTs, which are localized with respect to Au alignment markers by Scanning Electron Microscopy (SEM). A SEM picture of a typical device is shown in figure 1a. We fabricate our devices using standard e-beam lithography and thin film deposition techniques. We deposit the normal and the superconducting contact in one fabrication step using shadow evaporation techniques. The normal contacts consist of 5nm of titanium followed by 50nm of Au or of 70nm of Pd. The central superconducting electrode, 80nm – 100nm wide, is a Al(100nm)/Pd(3nm) bilayer. Such a method allows to achieve contact resistances as low as 30kOhm between normal and superconducting reservoir. In addition to the highly doped Si substrate with 500nm SiO_2 which is used as a global backgate, we implement two side gates whose voltage V_{SG1} and V_{SG2} can be tuned to control the two different parts defined by the central superconducting electrode. The spacing between the two normal contacts is between 600nm and 1.2 μm . All the measurements presented in this letter have been carried out in a dilution refrigerator with a base temperature of 80mK, on one particular sample which fulfilled the (stringent) requirements of double dot spectroscopy and high enough coupling to the superconducting electrode. The currents flowing through the different arms of the beam splitter are measured via the voltage drop across two 2k Ω resistors placed in series with the device as shown on figure 1a.

For characterization, we first operate the device as a series double quantum dot by setting $V_M = 0$ and $V_S \neq 0$ using the bias scheme shown in figure 1a. Figure 2a displays the color scale plot of linear conductance $G_L = dI_L/dV_S$ through the right (R) arm of the device as a function of side gate voltage 2 V_{SG2} and side gate voltage 1 V_{SG1} . The characteristic ‘honeycomb’ stability diagram of a double quantum dot with rather regularly spaced avoided crossings is observed.

For the remaining of the letter, we operate the device as a beam splitter by setting $V_M \neq 0$ and $V_S = 0$. The differential conductance corresponding to the left (L) arm and to the right (R) arm of the beam splitter have qualitatively the same dependence as a function of V_M , V_{SG1} or V_{SG2} . If V_{SG1} and V_{SG2} are tuned out of resonance, one typically measures a $G_L = dI_L/dV_M$ shown in figure 2b. This demonstrates tunneling into a superconductor i.e. the current is strongly suppressed for a bias voltage below the energy gap Δ . Such a feature has been used very recently to probe the quasiparticle relaxation time in SWNTs[18]. A fitting to the thermally smeared BCS density of states gives $\Delta = 85\mu eV$ and an electronic temperature of 100mK. Therefore, for $V_M < 85\mu eV$, one can only inject Cooper pairs. Note that the energy gap has a

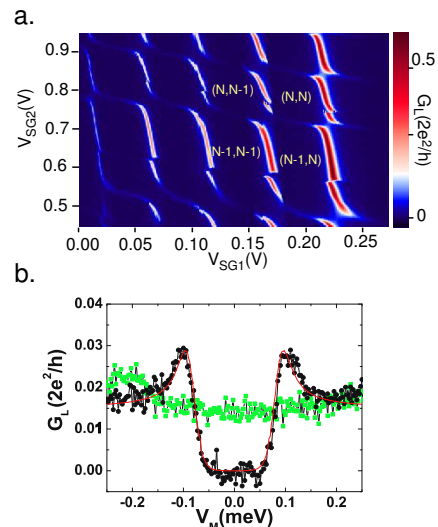


FIG. 2: a. Colorscale plot of the differential conductance G_L as a function of side gate voltage 1 V_{SG1} and side gate voltage 2 V_{SG2} . b. Differential conductance (black squares with lines) measured out of resonance in the middle injection scheme at 100mK and 0mT. In green square, the differential conductance at 44.5mT. In red solid lines, the BCS fit which yields an energy gap Δ of 85 μeV and an electronic temperature of 100mK.

reduced value with respect to pure Al since it corresponds to the minigap of the Al/Pd bilayer [19]. As shown on figure 2b in green squares, the BCS gap does not appear if a magnetic field of 44.5mT is applied perpendicularly to the axis of the superconducting finger. This allows us to define the normal (N) state of the beamsplitter for which we apply a field of 89mT in order to be sure that superconductivity of the Al/Pd slab is absent. The superconducting (S) state is obtained for 0mT.

The colorscale plot of figure 3a displays G_L for $V_M = 40\mu eV$ as a function of V_{SG1} and V_{SG2} for a specific anticrossing (AC1) in the S state. In contrast to the off resonance case shown in figure 2b, a relatively high subgap current $I_S \approx 0.1I_N$ can flow into or from the superconductor even though V_M is smaller than the energy gap at AC1. The presence of a subgap current can only be understood if Andreev reflections are taking place at resonance. In order to characterize the type of Andreev process occurring near the anticrossing, we show in figure 3b the variations of $G_L = dI_L/dV_M$ and $G_R = dI_R/dV_M$ measured simultaneously along the yellow arrow of the colorscale plot in figure 3a. In the N state (black solid lines), G_L and G_R display two peaks corresponding to the bonding/antibonding states of the double dot. Due to an asymmetry of the coupling of each dot to the L(R) reservoirs, the height of each doublet of peaks is different. In the S state represented in red solid lines, the peak height is reduced, but there is still a finite conductance for the L(R) arm which follows essentially the

resonances observed in the N state. A similar feature is shown in figure 3c for another anti-crossing (AC2) for which the asymmetry between G_L and G_R is slightly different. Note that the curves in the N state have been scaled down by $1/3$ for the sake of clarity.

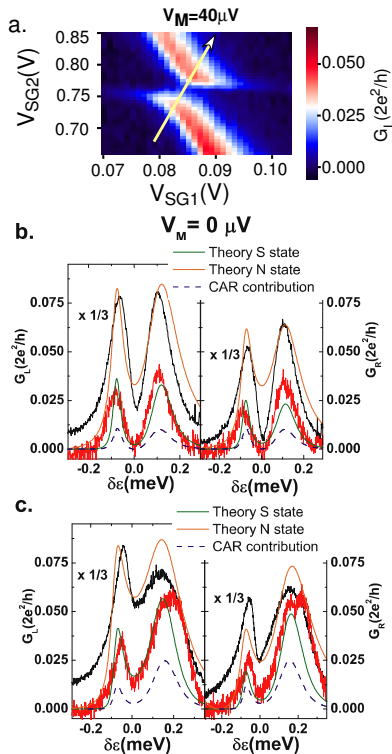


FIG. 3: a. Focus on a specific region for the differential conductance G_L as a function of V_{SG1} and V_{SG2} (AC1). The yellow arrow indicates the direction in which the linear scan of panel b. has been taken. b. Measurements of the conductance in the normal state (black solid lines) and in the superconducting state (red lines) for G_R and G_L along the direction of the yellow arrow. For the sake of clarity, the N state conductances have been multiplied by $1/3$. The model calculations are in green solid lines for the S state and in orange solid lines for the N state. In blue dashed lines, the CAR probability. c. Similar graph as in b. for anticrossing 2 (AC2)

The elementary processes which contribute to the sub-gap current in our double quantum dot setup at the degeneracy point are schematically sketched in figure 1b. The tunnel rates to the S,L and R contacts are respectively Γ_S , Γ_L and Γ_R . The initial state in the superconductor S is represented in blue and the final state in the normal metals N, in red. In process 1, two particles are transferred to the same reservoir and the corresponding probability is proportional to $\Gamma_{L,R}^2$. In processes 2 and 3 which are equivalent, one particle is transferred to each reservoir. The corresponding probability is therefore proportional to $\Gamma_L \Gamma_R$. While the beam splitter geometry imposes the above general form for the Andreev tunneling probabilities, our theory (which we discuss in detail in the EPAPS) allows to give an absolute value of the

proportionality constants of the AR and the CAR, by accounting for higher processes.

From the anti-crossing of figure 3a and the full stability diagram of figure 2a, we determine all the important parameters of the double dot using non-linear transport similarly to what is done in ref. 20 for example. The corresponding plots obtained from our theory at $T = 0$ are given in green solid lines for the S state and in orange solid line for the N state for two anticrossings AC1 and AC2. Each anticrossing is characterized by the set of parameters $\{U_L, U_R, \Gamma_{12}, \Gamma_L, \Gamma_R, \Gamma_{SL}, \Gamma_{SR}\}$, $U_{L,R}$ being the onsite charging energy, Γ_{12} the coupling between the two dots, Γ_L, Γ_R the coupling of each dot to its reservoir and Γ_{SL}, Γ_{SR} the coupling of the superconductor to each dot. Although not all of these parameters can be determined independently, the fitting establishes the following hierarchy of energy scales: $U_{L,R} \approx 1 \text{ meV}$, $\Gamma_{12} \approx 100 \mu\text{eV}$, $\Gamma_L, \Gamma_R \approx 100 \mu\text{eV}$ and $\Gamma_{SL}, \Gamma_{SR} \approx 10 \mu\text{eV}$. For both arms and both anticrossings, the calculated current in the superconducting state is in good agreement with our experimental findings, which implies an important contribution from CAR processes, as shown by the dashed lines in figure 3b and 3c. For AC1, for example, the fit allows us to extract a contribution of split Cooper pairs up to 35% for G_L and 55% for G_R .

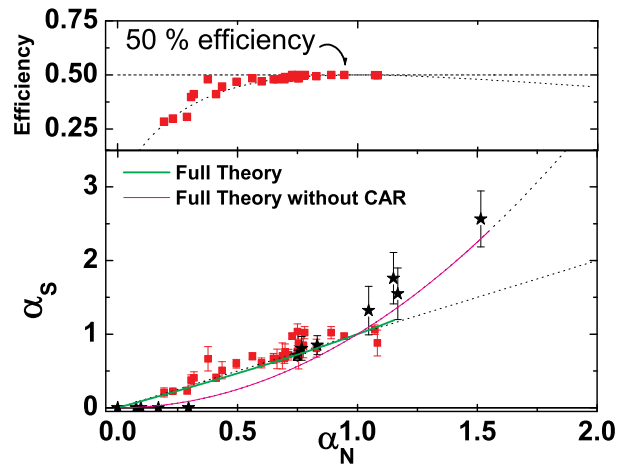


FIG. 4: Top panel : Efficiency of the Cooper pair splitting for the device. The solid green line corresponds to the asymmetry variation predicted by the interacting theory. Bottom panel : Asymmetry in the superconducting state versus asymmetry in the normal state for 31 out of the 35 anti-crossings studied (red closed squares) and 11 resonance peaks away from the anti-crossings (black stars). The dashed curve corresponds to $\alpha_S = \alpha_N^2$. The solid dashed line corresponds to $\alpha_S = \alpha_N$. The green line is the full theory (see EPAPS) and the pink line is the full theory without the CAR process.

Now, we exploit the asymmetry of transport between the L and R arms to provide further evidence for the

Cooper pair splitting. In the S state, it is defined as $\alpha_S = G_L/G_R$ at 0mT, and in the N state, as $\alpha_N = G_L/G_R$ at 89mT, both taken at resonance. One can already anticipate from the elementary processes of figure 1b that the presence or the absence of processes 2 and 3 should be observable directly from the dependence of α_S with respect to α_N . At the degeneracy point, both the local and non-local Andreev processes acquire a Breit-Wigner-like form at resonance (see EPAPS). In the limit $\Gamma_{12} \gg \Gamma_{L,R} \gg \Gamma_S$, obtain for the conductance $G_{L(R)}$:

$$G_{L(R)} = \frac{4e^2}{h} \frac{16\tilde{\Gamma}_S^2}{[\Gamma_L + \Gamma_R]^4} [\Gamma_{L(R)}^2 + \Gamma_L\Gamma_R], \quad (1)$$

where $\tilde{\Gamma}_S$ is the tunnel rate to the superconductor renormalized by Coulomb interactions. The presence of the crossed term $\Gamma_L\Gamma_R$ in equation (1) implies that:

$$\alpha_S = \frac{\Gamma_L^2 + \Gamma_L\Gamma_R}{\Gamma_R^2 + \Gamma_L\Gamma_R} = \frac{\Gamma_L}{\Gamma_R} = \alpha_N. \quad (2)$$

Away from the degeneracy points, when one of the dots is blocked, only local AR are present and the term proportional to $\Gamma_L\Gamma_R$ in equation (1) is absent. In this case, α_S is just the square of α_N . The bottom panel of figure 4 displays α_S versus α_N for all the anti-crossings which we have measured, in red squares, and resonances away from the anticrossings, in black stars. The 31 red squares correspond to 7 different anticrossings. The error bars correspond to the systematic error made when determining α_S . The black stars are obtained when one of the two dots is Coulomb blockaded (single resonance case). Within the error bars, they fall onto the dashed curve which corresponds to the universal parabola $\alpha_S = \alpha_N^2$ as expected. The red points fall onto the universal dashed line $\alpha_S = \alpha_N$ [21]. The observed contrast between the quadratic behavior followed by the black stars and the linear behaviour followed by the red squares proves the Cooper pair splitting action of our device. Note that the full theory (i.e. without the approximations leading to Eq. (1)) predicts a dependence of α_S versus α_N which is marginally different from these behaviors in our parameter range as shown by the green and pink curves in figure 4. The universal linear behavior arising from the Cooper pair splitting is therefore a very useful diagnosis tool for a wide range of parameters of our beam splitter. The efficiency of the beam splitter can be defined as the ratio $2T_{CAR}/(AR_L + AR_R + 2T_{CAR}) \approx 2/(2 + 1/\alpha_S + \alpha_S)$ of the split current to the total current. It is displayed on the top panel of figure 4. For a α_N ranging from 0.5 to 1, the efficiency of Cooper pair splitting is close to 50%, showing that almost half of the Cooper pairs flowing out of the superconducting finger are split at the SWNT.

In conclusion, we have shown that carbon nanotube double quantum dots can be used as tunable Cooper pair beam splitters. The specific advantage of beam splitters based on double quantum dots is the possibility of further

processing the electron states e.g. by spin filtering for EPR type experiments.

During the course of writing this paper, we became aware of a similar study using InAs nanowires by Hofstetter et al.[22].

We thank A. Cottet for a critical reading of the manuscript and illuminating discussions. We thank The Mesoscopics group of LPA, The Quantronics Group and J. Siewert for assistance and fruitful discussions. This work is supported by the SFB 689 of the Deutsche Forschungsgemeinschaft, the ANR-05-NANO-028 contract, the ANR-07-NANO-011-004 contract, the EU contract FP6-IST-021285-2, the C'Nano Ile de France contract SPINMOL, the Spanish MICINN under contract FIS2008-04209 and the DFH-UFA and DAAD mobility grants.

-
- [1] G. Fève, A. Mahé, J.-M. Berroir et al., *Science* **316**, 1169 (2007).
 - [2] A. Wallraff, D.I. Schuster, A. Blais et al., *Nature* **431**, 162 (2004).
 - [3] N.M. Chtchelkachev, G. Blatter, G.B. Lesovik and T. Martin, *Phys. Rev. B* **66**, 161320(R) (2002).
 - [4] P. Samuelsson, E.V. Sukhorukov and M. Büttiker, *Phys. Rev. Lett.* **91**, 157002 (2003).
 - [5] T. Martin *Phys. Lett. A* **220**, 137 (1996).
 - [6] P. Recher, E.V. Sukhorukov and D. Loss, *Phys. Rev. B* **63**, 165314 (2001).
 - [7] G. B. Lesovik, T. Martin and G. Blatter, *Eur. Phys. J. B* **24**, 287 (2001).
 - [8] S. M.-S. Choi, C. Bruder, and D. Loss, *Phys. Rev. B* **62**, 13569 (2000).
 - [9] P. Recher and D. Loss *Phys. Rev. B* **65**, 165327 (2002).
 - [10] C. Bena, S. Vishveshwara, L. Balents and M.P.A. Fisher, *Phys. Rev. Lett.* **89**, 037901 (2002).
 - [11] V. Bouchiat, N. Chtchelkatchev, D. Feinberg *et al.*, *Nanotechnology* **14**, 77 (2003).
 - [12] A. Levy Yeyati, F.S. Bergeret, A. Martín-Rodero and T.M. Klapwijk, *Nature Phys.* **3**, 455 (2007).
 - [13] E. Dupont and K. Le Hur, *Phys. Rev. B* **73**, 045325 (2006).
 - [14] D. Feinberg and G. Deutscher, *Appl. Phys. Lett.* **76**, 487 (2000).
 - [15] J. Cayssol, *Phys. Rev. Lett.* **100**, 147001 (2008).
 - [16] D. Beckmann, H.B. Weber and H. v. Lhneysen, *Phys. Rev. Lett.* **93**, 197003 (2004).
 - [17] S. Russo, M. Kroug, T.M. Klapwijk and A.F. Morpurgo, *Phys. Rev. Lett.* **95**, 027002 (2005).
 - [18] Y.-F. Chen, T. Dirks, G. Al-Zoubi, N.O. Birge and N. Mason, *Phys. Rev. Lett.* **102**, 036804 (2009).
 - [19] T. Kontos, M. Aprili, J. Lesueur, X. Grison and L. Dumoulin, *Phys. Rev. Lett.* **93**, 137001 (2004).
 - [20] M. Gräber, W.A. Coish, C. Hoffmann et al., *Phys. Rev. B* **74**, 075427 (2006).
 - [21] As we discuss in the EPAPS we do not include in figure 4 points corresponding to 2 anticrossings for which the condition $\Gamma_{L,R} \gg \Gamma_S$ did not apply and which were anomalously sensitive to detuning. It should be men-

tioned, however, that they can be fully accounted by the full theory, as shown in the EPAPS

[22] Hofstetter L., Csonka S., Nygard J. and Schönenberger

C., submitted.